Available online at www.sciencedirect.com
ScienceDirect
International Journal of Mass Spectrometry 265 (2007) 372–381
International Journal of Mass Spectrometry
www.elsevier.com/locate/ijms

Collision energetics in a tandem time-of-flight (TOF/TOF) mass spectrometer with a curved-field reflectron

Serguei Ilchenko [1], Robert J. Cotter *

Middle Atlantic Mass Spectrometry Laboratory, Department of Pharmacology and Molecular Sciences, The Johns Hopkins University School of Medicine, Baltimore, MD 21205, United States

Received 24 October 2006; received in revised form 30 May 2007; accepted 3 June 2007
Available online 9 June 2007

Abstract

Collisions of fullerene ions (C_{60}^+) with helium and neon were carried out over a range of laboratory energies (3–20 keV) on a unique tandem time-of-flight (TOF/TOF) mass spectrometer equipped with a curved-field reflectron (CFR). The CFR enables focusing of product ions over a wide kinetic energy range. Thus, ions extracted from a laser desorption/ionization (LDI) source are not decelerated prior to collision, and collision energies in the laboratory frame are determined by the source extraction voltages. Comparison of product ion mass spectra obtained following collisions with inert gases show a time (and apparent mass) shift for product ions relative to those observed in spectra obtained by metastable dissociation (unimolecular decay), consistent with impulse collision models, in which interactions of helium with fullerene in the high energy range are primarily with a single carbon atom. In addition, within a narrow range of kinetic energies an additional peak corresponding to the capture of helium is observed for fragment ions C_{50}^+, C_{52}^+, C_{54}^+, C_{56}^+ and C_{58}^+.

Keywords: Collision energetics; Fullerenes; Impulse collision theory; Curved-field reflectron; Time-of-flight mass spectrometry

1. Introduction

Collision-induced dissociation (CID) is one of the methods used in many different types of mass spectrometers to produce structurally informative fragmentation. The collision process and the transfer of kinetic energy to internal energy of the projectile ion have undergone detailed investigation and are better understood for small molecules [1,2]. The dissociation of large molecules is complicated by the increase in the number of degrees of freedom, which restrict the rate of dissociation and the fragment ion yield [3]. To increase the relative collision energy (in the center-of-mass frame) and the internal excitation energy, it is common to use higher acceleration voltages and heavier target gases; however, it has been noted that the lower ionization potential and the lower energy between excited and ground electronic states of heavier noble gases results in their excitation as well, thus decreasing the energy available for transfer to the analyte ion [4–7]. Another consequence of this additional inelasticity is that heavier target atoms result in a somewhat smaller shift in the velocity of the parent ion (and fragment ions) than would be expected solely from consideration of their relative collision energy and excitation of the projectile molecular ion [8]. In the time-of-flight (TOF) mass spectrometer, collisions with a target gas will result in fragment ions with longer arrival times than their counterparts resulting from unimolecular (or post-source) decay. These shifts in arrival times (expressed as shifts in apparent mass) are used here to probe the mechanisms involved in very high energy collisions by comparing the experimental results with those predicted from impulse collision models [9,10].

In the case of the spherical fullerene C_{60} molecule it is also possible to capture different targets [10–24]. For noble gas atoms this interaction does not involve the formation of a chemical bond. The atom penetrates the fullerene sphere, losing sufficient energy in the process to prevent its escape. The threshold for penetration of He through a six-membered ring of C_{60} has been evaluated as 9.35 eV, and through a five-membered ring as 13.1 eV [13], while the decomposition energy

* Corresponding author. Tel.: +1 410 955 3022; fax: +1 410 955 3420.
E-mail address: rcotter@jhmi.edu (R.J. Cotter).
[1] Current address: Center for Proteomics, Case Western Reserve University, Cleveland, OH 44106, United States.

1387-3806/$ – see front matter © 2007 Elsevier B.V. All rights reserved.
doi:10.1016/j.ijms.2007.06.006

of C_{60}^+ with C_2 loss has been evaluated as 7.0–7.6 eV [14,16]. A molecular dynamics simulation predicts the maximum yield at a laboratory collision energy of 8 keV [13], though the maximum yield in our experiments (see below) was observed at 6 keV (33 eV in the center-of-mass frame) [12]. Most of the experiments involving high-energy collisions of fullerenes have been carried out using sector instruments or time-of-flight mass spectrometers combined with a retarding field energy analyzer [10–13,16–18,20,21]. In this investigation we detect helium-trapped fragments using a unique time-of-flight mass analyzer with a curved field reflectron. In this case, it is not necessary to decelerate the ions to very low kinetic energies prior to collision in order to accommodate the focusing bandwidth of the reflectron [25]; therefore, it is possible to investigate a wide range of collision energies by simply reducing the initial acceleration voltage. Within each single spectrum we detected metastable, CID and (for lower collision energies) trapped helium fragments, from which we determined the time (apparent mass) shifts that enabled us to assess the different types of collisions based on impulse collision theory (ICT) [9].

2. Experimental

Tandem mass spectra were obtained on a Kratos (Manchester, England) AXIMA CFR time-of-flight mass spectrometer modified, as described previously [26,27], with a collision cell mounted at the top of the ion source and ion focusing optics in the region ahead of the mass selection gate (Fig. 1). The collision chamber is a stainless steel cylinder (1.13 in. long, 0.2 in. i.d.) and the collision gas is injected into the chamber through a long (2 m) 0.07 mm i.d. glass capillary tube at a flow rate of 0–1 ml/min. The collision gas pressure in the chamber cannot be measured directly, so that the vacuum chamber pressure (Torr) was monitored to insure reproducible conditions. The experiments reported here were carried out at pressures which we have shown earlier from pressure dependence measurements on this instrument to correspond to primarily single-collision conditions [25]. The normal acceleration energy for ions in this instrument is 20 keV. In order to carry out collisions over a wide range of (laboratory) collision energies, including those that would permit capture of helium, the acceleration voltage was varied in the range from 3 to 20 kV. The ion extraction field, Einzel lens, deflector and reflector voltages were changed proportionally and then adjusted to optimize ion beam focusing on the detector. Data was first acquired in the linear TOF mode, which does not reveal the fragment ions, but permits more direct assessment of the difference in velocity of the molecular ions that have and have not undergone collisions. In the reflectron mode experiments, with or without a target gas, the peaks corresponding to the parent ion C_{60}^+ and fragments arising from unimolecular (metastable) processes were detected and used for mass calibration. The time delay was unchanged in all experiments and equal to 100 ns.

Buckminsterfullerene C_{60} was obtained from Aldrich (Milwaukee, WI) and used without further purification. 0.5 μl of saturated solutions of C_{60} in benzene (Baker, Inc., Phillipsburg, NJ) were transferred directly to the sample plate and allowed to dry. Substance P was obtained from Sigma Chemical (St. Louis, MO). High purity helium and neon (99.999%) were obtained from BOC Group, Inc. (Murray Hill, NJ).

The target gas density inside the collision cell was estimated to be about two orders of magnitude higher than the density in the acceleration chamber, based upon previous measurements of the beam attenuation. The pressure of residual gas in the source chamber did not exceed 0.5 μTorr when no target gas was used, and up to 10 μTorr with the target gas. However, the parent-gas interactions outside of the collision chamber appeared to lead to negligible reduction in mass resolution. Some scattering losses were observed, primarily at low collision energies. Spectra were averaged over 100 shots. It should be noted that in our preliminary experiments it was found that fullerene fragmentation yield is increased several times as the laser irradiation is changed on our instrument from 50 to 60 (attenuator units). Thus, ions desorbed by the laser will carry considerable internal energy, which could decrease the effective dissociation energy to less than 10 eV. A sample plate was moved step by step so that each laser pulse hits a new spot of a sample, which is important for the reproducibility of the plume density and the ion internal energy.

3. Impact collision theory

Collision induced dissociation (CID) is essentially a two step process that involves excitation of a precursor ion upon impact with a target atom or molecule (usually an inert gas atom), followed by cleavage of chemical bonds in the ion to form separated ionic and neutral fragments [1–3,9]. After an elastic collision the precursor ion and target atom fly apart with velocities and kinetic energies that are different from their initial ones, but which conserve the center-of-mass velocity of the system. No contribution is made to changing the internal energy, so that

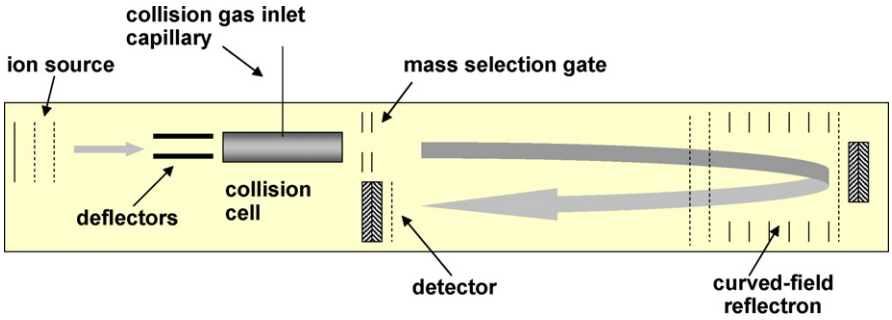

Fig. 1. Schematic diagram of the modifications to the TOF/TOF mass spectrometer with a curved-field reflectron showing the location of the collision chamber.

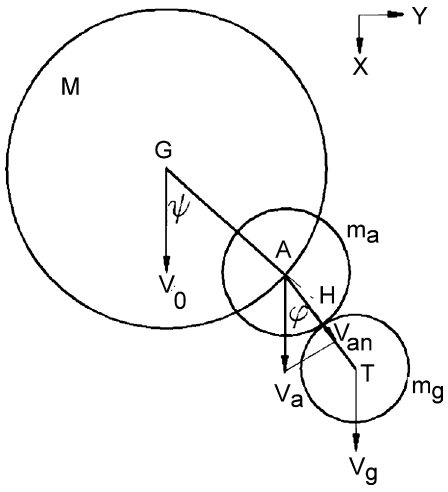

Fig. 2. Diagram of the impulsive collision model showing the impact angle φ between the target atom m_g and a carbon atom m_a. The angle ψ shows the position of m_a in the fullerene M with respect to the direction of velocity.

an elastic impact would not itself be responsible for inducing ion dissociation. However, the product ions m_p resulting from metastable dissociation of already activated precursor ions after an elastic collision would have velocities and kinetic energies that are slightly different from metastable products formed in the absence of a collision.

3.1. The initial interaction

For large biological molecules the initial impact occurs more locally, between the target atom (usually a noble gas) and only one atom m_a or group of atoms of the projectile. The simplest case of the so-called impact collision theory (ICT), described by Uggerud and Derrick [9], involves an initial elastic impact of the target atom with m_a, which then interacts with the remaining ion with full inelasticity, predicting an ion velocity and kinetic energy:

$$V_{ICT} = V_0 \frac{M(m_g + m_a) - 2m_g m_a \cos^2\varphi}{M(m_g + m_a)} \quad (1)$$

$$T_{ICT} = T_0 \left(\frac{M(m_g + m_a) - 2m_g m_a \cos^2\varphi}{M(m_g + m_a)} \right)^2 \quad (2)$$

where V_0 and T_0 are the initial ion velocity and kinetic energy, respectively, and φ is the initial impact angle (Fig. 2). In this case the increase in internal energy of the projectile molecules is

$$\Delta Q_{ICT} = T_0 \frac{4m_a m_g^2 (M - m_a)}{(m_g + m_a)^2 M^2} \cos^2\varphi \quad (3)$$

A more complete picture of ICT includes the possibility for excitation of the target gas in the initial collision [5,6] and depends upon the target ionization potential and excited electronic states (e.g., 19.8 eV for He and 16.6 eV for Ne). In this case the initial interaction of target gas with the effective mass m_a is partially elastic, and it is convenient to characterize the interaction by a restitution coefficient k that ranges from 1 (elastic) to 0 (fully ineleastic) (see Ref. [28] and Appendix 2). As was noted in Ref. [21] existing molecular dynamic simulations of collisions are valid when electronically excitation is negligible. The present approach is an effort to take into account this excitation, though not its specific dependence on the ionization potential. The restitution parameter is unknown, but might be determined empirically by evaluating experimental data for shifts in arrival times in line with this model.

3.2. The second interaction

If as described above the second step is inelastic and the first partially elastic, the parent velocity along the x-axis (or original direction of travel) would be

$$V_{ICT,inelastic} = V_0 \frac{M(m_g + m_a) - (1 + k_1) m_g m_a \cos^2\varphi}{M(m_g + m_a)} \quad (4)$$

while the velocity in the y direction is important in evaluating the scattering angle, the internal energy excitation of the parent ion maybe written as

$$\Delta Q_{ICT,inelastic} = T_0 \frac{(1 + k_1)^2 m_a m_g^2 (M - m_a)}{(m_g + m_a)^2 M^2} \cos^2\varphi \quad (5)$$

where these expressions reduce to the simpler ICT case when $k_1 = 1$. Shukla and Futrell [2] have considered the case when the second step of ICT is a knockout impact, while the first is elastic. Here, we consider that both steps are partially elastic, but in the second step the atom m_a is knocked out of the ion. The final velocities in the x and y directions are defined by the restitution coefficient k_2 and the angle position ψ of m_a in the parent ion (Fig. 2). Along the flight direction (x-axis) the velocity is

$$V_{ICT,knockout} = V_0 \frac{M(m_g + m_a) - (1 + k_1)(1 + k_2) m_g m_a \cos\varphi \cos\psi \cos(\varphi - \psi)}{M(m_g + m_a)} \quad (6)$$

and the internal energy of the ion and m_a is

$$\Delta Q_{ICT,knockout} = T_0 \frac{(1 - k_2^2)(1 + k_1)(M - m_a) m_a m_g^2}{M^2 (m_g + m_a)^2} \times \cos^2\varphi \cos^2(\varphi - \psi) \quad (7)$$

3.3. Fragment (product) ions

For decompositions of the type $M^+ \rightarrow m_p{}^+ + m_n$, induced by the different processes described above, the ion m_p and neutral m_n fragments will have close to the same translational velocities

as their precursor ions, but their kinetic energies are proportional to their respective fractional masses.

3.4. Evaluation of ion flight times for each process

The time-of-flight (TOF) for any ion includes the times spent in the source, the drift space L and the reflectron, in this case a curved-field reflectron (CFR). The potentials defining the electric field in the CFR may be presented by the linear and quadratic terms of a longitude coordinate x if any higher field harmonics are negligible [29]: $U(x) = ax^2 + bx$, so the TOF of the ion with kinetic energy T is calculated by

$$t_{\mathrm{CFR}} = 2\int_0^d \left(\frac{2e}{m}\right)^{-1/2} (T - ax^2 - bx)^{-1/2}\,\mathrm{d}x$$
$$= 2\left(\frac{m}{2ea}\right)^{1/2}\left(\frac{\pi}{2} - \arcsin\left(\frac{1+4aT}{b^2}\right)\right)^{-1/2} \quad (8)$$

Here the integral limit d is the penetration depth when $U(d) = T$:

$$d = -\frac{b}{2a} + \left(\frac{b^2}{4a^2} + \frac{T}{a}\right)^{1/2} \quad (9)$$

If the quadratic component of the field is small ($aT/b^2 \ll 1$) one may expand Eq. (8) to

$$t_{\mathrm{CFR}} = 2\left(\frac{m}{2ea}\right)^{1/2}\left(\frac{(4aT/b^2)}{(1+4aT/b^2)}\right)^{1/2}$$
$$= 2\left(\frac{2mT}{eb^2}\right)^{1/2}\left(\frac{1+4aT}{b^2}\right)^{-1/2} \quad (10)$$

For a linear reflectron ($a = 0$), one may obtain simple expressions for elastic and inelastic head-on collisions, impulsive collisions (ICT) and metastable fragmentation (see Appendix 1). Analysis of the flight times for these different collision models (A1)–(A6) in an instrument with a linear reflectron (or $a \ll b$) predicts that fragments produced in collisions with a heavier target would be characterized by longer flight times than those produced with a light target. Increasing the quadratic coefficient a for the field curvature (for the CFR) leads to an increase in time shifts, but the relative shifts involving light and heavy targets is still the same.

The two step processes involving inelastic or partially elastic second collisions lead to further decreases in the loss of kinetic energy compared to ICT (thereby narrowing further the time difference when compared to unimolecular decomposition). The equations for describing the TOF for these processes are cumbersome expressions; however, it is convenient to calculate the TOF using Eq. (8) directly by substituting the appropriate velocity and kinetic energy described by Eqs. (4)–(7).

For an accurate analysis and comparison with observed data, however, it is necessary to evaluate the actual field curvature in the CFR. This was accomplished empirically by measuring the flight times of a test species as the reflectron voltage was changed in intervals ±2 kV from the nominal value. No gas was present in the collision cell and the acceleration voltage was unchanged, so that the times spent in the extraction and drift regions are constant

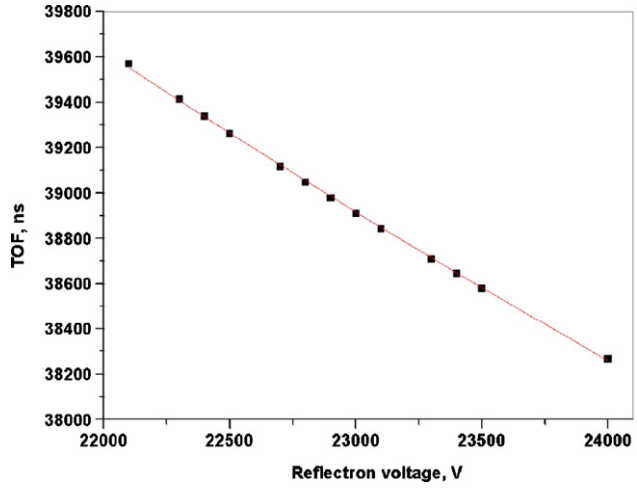

Fig. 3. Measured flight times for substance P vs. the voltage on the curved-field reflectron used to map the quadratic electric field in the reflectron by fitting the equation: $U(x) = ax^2 + bx$.

and the variation in the time spent in the reflectron could be used to find the coefficients a and b that provide the best fit between the experimental data and Eq. (8). The ion kinetic energy T is assumed to be less than the acceleration energy for 20–50 eV as a result of the expansion of the laser evaporated plume during a time delay of 100 ns. (The speed of plume is assumed to be about 500–900 m/s [30–35], and the electric field strength in the extraction acceleration gap is evaluated as 450–500 V/mm.) Thus, using the fitting method of ORIGING6, the TOF data for fullerene and substance P (Fig. 3) give an estimate of a as 2.7 ± 0.2 and b as 1.85 ± 0.07.

The flight times evaluated for simple elastic and inelastic processes using Eq. (8) for the CFR are shown in Fig. 4a as a mass shift relative to fragments with the same mass, but produced in a metastable process. It should be noted that the time scale is proportional to the mass in the vicinity of fragment with any mass $M - m_{\mathrm{n}}$. This allows us to convert the calculated time difference $(t_{\mathrm{in}} - t_1)$ for any process i into a mass scale dm_{in} using the relationship: $dm_{\mathrm{in}} = 4[\mathrm{Da}]\ (t_{\mathrm{in}} - t_1)/(t_{\mathrm{n4}} - t_{\mathrm{n}})$, where t_{n4} and t_{n} mean calculated flight time of PSD fragments with mass release of $(m_{\mathrm{n}} - 4)$ and m_{n} accordingly. The units on the abscissa correspond to the masses of neutral fragment m_{n} released from the parent ion. The calculations were made for an acceleration voltage at 6 kV, the location of the collision cell at 10 cm, a drift space of 80 cm, and reflectron field curvature parameters as estimated above.

4. Results and discussion

4.1. Collision-induced dissociation versus post-source decay

Tandem mass spectra were obtained for the product ions formed from fullerene C_{60} with no collision gas, with helium and with neon, over a range of ion accelerating energies from 3 to 20 keV. Without a collision gas only the C_{58}^+ fragment is

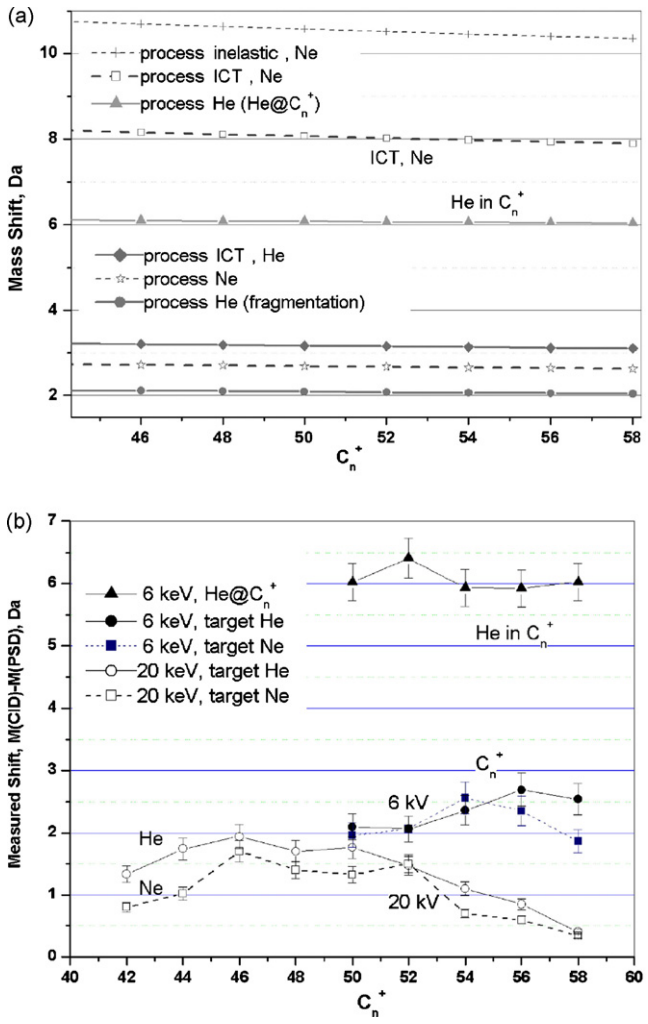

Fig. 4. (a) Expected shifts in apparent mass for the C_n^+ ions formed from collisions of C_{60}^+ with helium or neon calculated using a simple elastic collision model and impact collision theory. (b) Experimental apparent mass shifts for the C_{2n}^+ and $C_{2n}He^+$ fragments formed by collisions of C_{60}^+ with helium, and the C_{2n}^+ fragments formed by collisions with neon at collision energies of 6 and 20 keV.

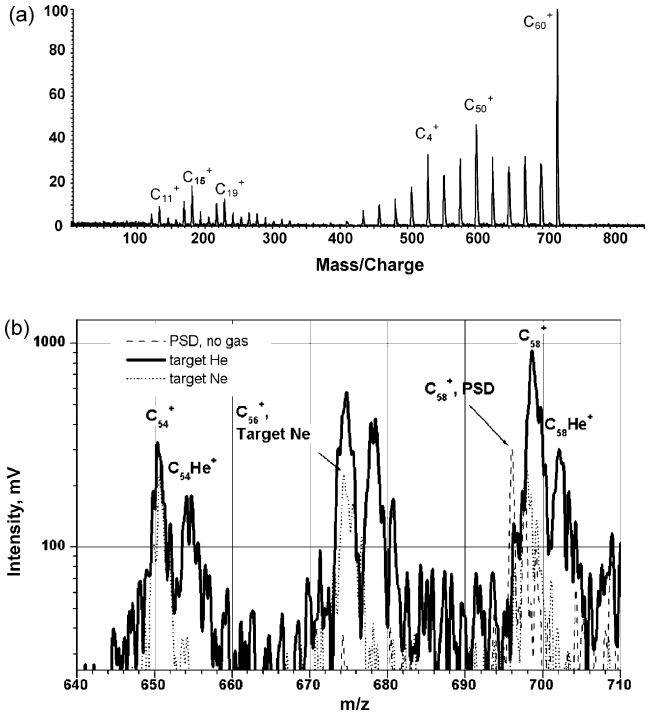

Fig. 5. (a) Tandem 20 keV CID mass spectrum of C_{60}^+ with helium. Gas pressure in the drift chamber is 2.5×10^{-5} Torr. (b) MS/MS spectra of fullerene obtained by PSD or by CID with helium or neon target gas.

visible [25,36]. An MS/MS spectrum of fullerene with helium, at high attenuation and at 20 keV, is shown in Fig. 5a. The major ions in the upper mass region are the even-carbon species from C_{34}^+ to C_{58}^+, with the lower mass ions arising from multiple collisions [26]. In order to insure that only single collisions were involved in these experiments, the collision gas pressure was adjusted to the point that only the ions C_{42}^+–C_{58}^+ were observed in the 20 keV spectra. Under these conditions the fragment ion signal was reduced somewhat, particularly at the lower kinetic energies in which generally only the C_{50}^+–C_{58}^+ ions could be observed. Fig. 5b shows the metastable, He and Ne collision spectra at 6 keV over the range of C_{54}^+–C_{58}^+. In the He collision spectrum $C_{54}He^+$, $C_{56}He^+$ and $C_{58}He^+$ are also observed. These additional peaks are seen in all of the He collision spectra from 4 to 8 keV, and previous results from sector instruments [10–14] have suggested that they result from initial capture of He by C_{60}^+, and subsequent fragmentation. The maximum yield was observed at 6 keV (33 eV in the CM frame) [13], while a previously reported molecular dynamics simulation predicted the maximum around 8 keV [13]. No adducts with neon were observed.

4.2. Comparison with models

Using the C_{58}^+ and C_{60}^+ ions for mass calibration, the apparent mass shifts were determined for all of the collision-induced fragment ions and are shown in Fig. 4b for the C_{42}^+–C_{58}^+ ions at 20 keV, and for the C_{50}^+–C_{58}^+ and $C_{50}He^+$–$C_{58}He^+$ ions at 6 keV. Comparison with Fig. 4a shows that there is good correspondence between experiment and calculations (around 0.5 Da) when helium is the target gas. The apparent mass shift accompanying the formation of C_nHe^+ is consistent with the lower velocity expected following the capture of helium, while the shifts for C_n^+ may be described by ICT or a simple elastic collision in which a portion of the kinetic energy is partitioned to the helium atom. In the Ne case there is considerable apparent discrepancy between theory and experiment. Mass (time) shifts for neon predicted by ICT are nearly 5 Da greater than observed by experiment; indeed the shift for Ne is less than for He in all experiments at any reflectron voltage (6 or 20 kV), while the theory predicts that this should be just the reverse for a heavier target. This discrepancy suggests that the loss in parent ion kinetic energy is much less than would be predicted by a simple ICT model for collision with neon, which does not take into account the excitation of the target gas.

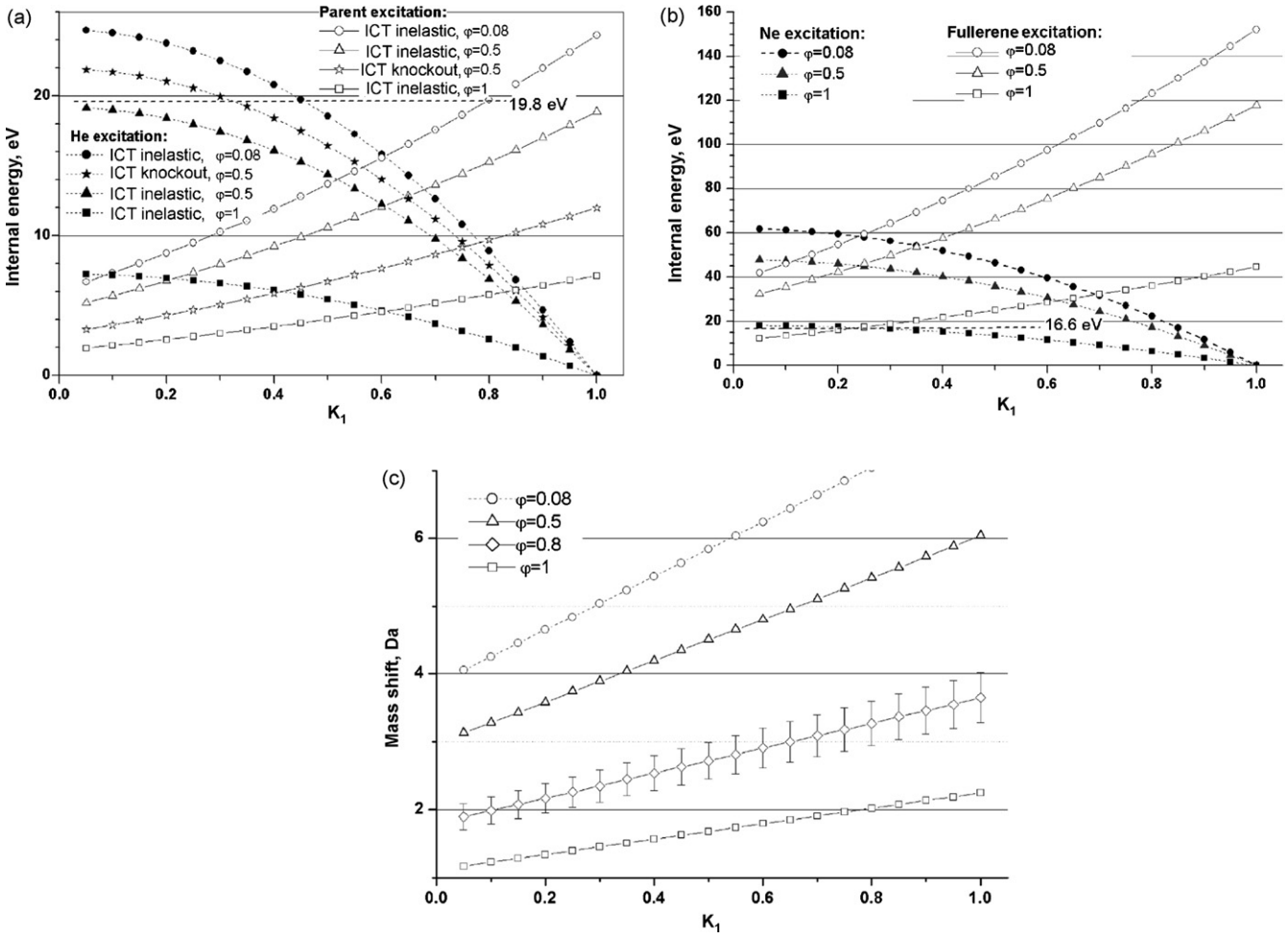

Fig. 6. (a) Calculated excitation of helium and C_{60}^+ by collisions C_{60}^+ with helium at 6 keV vs. restitution coefficient k_1 for different collision processes and different impact angles φ. (b) Calculated excitation of neon and C_{60}^+ at collision energy 6 keV vs. restitution coefficient k_1 for ICT inelastic process at different impact angles φ. (c) Calculated mass shifts resulting from excitation of C_{60}^+ by collisions with neon at 6 keV versus restitution coefficient k_1 for ICT inelastic collision process and different impact angles φ.

4.3. Comparison with partially elastic impact and knockout models

Thus, at least two factors could reduce the kinetic energy loss: a large impact parameter and/or inelastic scattering, both of which processes we had considered above. The latter includes possible internal excitation both for the projectile and for the target, for example, when the first step is partially elastic and the second is inelastic. Fig. 6a shows the conversion at 6 keV from collision energy to internal energy of both the helium target and the projectile molecule as a function of the restitution coefficient, $k_1 = 0$ (inelastic) to 1 (elastic), for the first collision step with m_a. Each of the curves represents a different impact parameter φ varying from 0.08 (nearly head-on) to 1.0 rad (glancing). Thus, for example, the curve for the impact parameter $\varphi = 0.08$ shows a complete conversion into internal energy of the target gas (around 24 eV) for a completely inelastic first interaction. This decreases with increasing elasticity and, since more kinetic energy becomes available for the second step, the conversion to internal energy of the precursor ion increases at higher elasticity. For higher impact parameters, the conversion to internal energy of both particles decreases, and the curves are considerably flatter. Fig. 6a also shows that at an impact angle $\varphi = 0.08$, $k_1 < 0.45$ would be required to excite the electronic state of He (19.8 eV) in its interaction with m_a, leaving a relatively small energy ($Q < 12$ eV) for excitation of the remaining fullerene ion. While the dissociation energy to form the fragment C_{58} (7.3 eV) is exceeded for $k_1 > 0.1$, the fragmentation of the parent ion would have low probability for such inelastic collisions, occurring only for very low impact parameters (direct hits). Indeed, for observation of fragments C_{56}^+–C_{50}^+ the internal energy must exceed about two to three times the energy needed for release C_2 [14]. In the case when $k_1 = 1$ (first elastic impact) the excitation energy would be 24 eV and the dissociation becomes considerably more probable. In addition, the calculated shifts for $k_1 < 0.45$ are in disagreement with the observed data (see below), so one may conclude that at parent ion energies of 6 keV, the fragmentation occurs rather via first elastic collisions with He. It should be noted that the molecular parameters, such as ionization potential and dissociation energy are not strongly affected in our model, though they may affect the range of restitution parameter k_1 for which fragmentation occurs.

The excitation dependences for the knockout impact mechanism are similar and are also shown in Fig. 6a. In this case the helium acquires slightly more energy (because the knockout mass m_a is taken as 24 Da, consistent with the experimental observation of even-carbon fragments), which increases the colliding energy. As a result the parent excitation is lower than the inelastic case, so that neither of these processes (which begin with a first inelastic step) would appear to play a role in the fragmentation. At the same time we have noted that the formation of fragments C_{2n}^+ following collision with helium (Fig. 4a) shows a good correspondence with the experimental data (Fig. 4b). Further support for that mechanism was obtained by scanning the (±5 Da width) mass selection gate across the molecular ion. Our observation shows that the ratio $[C_{2n}He^+]/[C_{2n}^+]$ remains constant (data not shown) suggests that both types of fragment ions traverse the gate with the same velocities and are thus formed from the same complex, He at C_{60}^+, in accordance with [12].

The situation is very different when Ne is used as the collision gas. As shown in Fig. 6b, the target excitation in a first inelastic step exceeds the excitation threshold of 16.6 eV over a wide range of inelasticities k_1. Parent ion excitation exceeds 30 eV, so the fragmentation is possible for impact parameter up to $\varphi = 1$. Fig. 6c shows the mass shifts calculated as a function of restitution coefficient k_1 for different impact angles φ corresponding to the parameters plotted in Fig. 6b. The calculated mass shifts for collision with neon with a first partially elastic step provides good agreement with the 2.2 Da experimental shift over a range impact angles ($0.6 < \varphi < 0.8$) and inelasticities ($0.2 < k_1 < 0.5$).

4.4. 20 keV collision energy

At a projectile ion kinetic energy of 20 keV processes in which the first step is partially elastic, second is inelastic or knockout give considerably more excitation both for the target and parent particles, which make these processes possible over wide range of k and impact angle φ for both He (Fig. 7a) and Ne (Fig. 7b). Focusing on one set of conditions, Fig. 7a shows that if the impact angle is 0.5 rad helium target excitation exceeds 19.8 eV for $k_1 < 0.85$, a nearly elastic first step. At the same time the fullerene excitation (when the second step is inelastic) that would exceed the energy (7.3 eV) required for dissociation leading to the loss of a C_2 fragment for $k_1 > 0.2$ even if $\varphi = 0.8$ could occur for a wide range of impact angle and restitution coefficient. However, the mass shift in agreement with the experiment data

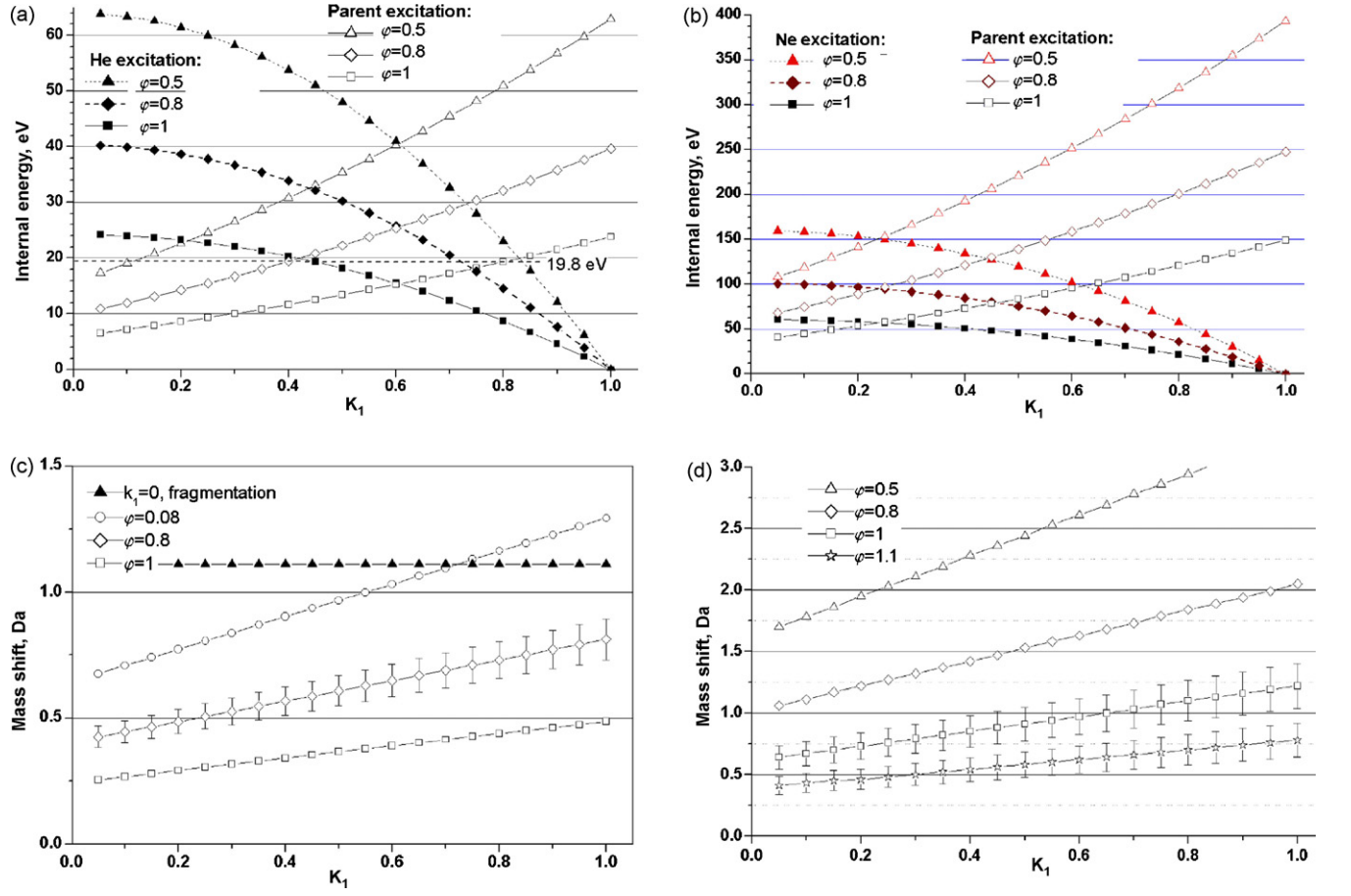

Fig. 7. (a) Calculated excitation of C_{60}^+ by collisions with helium at 20 keV vs. restitution coefficient k_1 for ICT inelastic collision process and different impact angles φ. (b) Calculated excitation of C_{60}^+ by collisions with neon at 20 keV vs. restitution coefficient k_1 for ICT inelastic collision process and different impact angles φ. (c) Calculated mass shifts resulting from excitation of C_{60}^+ by collisions with helium at 20 keV vs. restitution coefficient k_1 for ICT inelastic collision process and different impact angles φ. (d) Calculated mass shifts resulting from excitation of C_{60}^+ by collisions with neon at 20 keV vs. restitution coefficient k_1 for ICT inelastic collision process and different impact angles φ.

(0.4 Da) shows a somewhat narrower interval of $0.3 < k_1 < 0.6$ if $0.7 < \varphi < 0.9$ (Fig. 7c). Thus, an interaction in which the first step is a partially inelastic impact may explain the value of the mass shift. The interaction when the second step is a knockout process is possible as well; it would be in agreement with experiment for the larger impact angle of about 1 rad.

In the case of neon (Fig. 7b) the target excitation is more effective than for helium ($k_1 < 0.9$), while parent excitation is still high and fragmentation extensive. Excitation of Ne of more than 100 eV is not feasible, so small values of k_1 should be excluded. The agreement with experiment for mass shift of C_{58}^+ (0.4–0.5 Da) would be only for relatively high impact parameters (φ is about 1.1). Smaller φ leads to more energy transfer and induces larger mass shifts, which would be in better agreement with the experimental results for fragments C_{56}^+ and below (Fig. 7d).

Indeed, it is important that the yield of the fragments depend upon the internal energy, which depends upon impact angle. According to RRKM theory [2,3] the unimolecular dissociation rate has a threshold E_0. For a rough estimate the Arrhenius law maybe used [15]:

$$N_{i\varphi} = N_{0\varphi} \exp\left(-\frac{E_0}{Q_{i\varphi}}\right) \tag{11}$$

Here, index φ means the value connected with impact angles φ. The amount of the collisions at these angles depends on scattering angle and maybe expressed as

$$N_{0\varphi} = \cos\varphi \sin\varphi \, d\varphi = \frac{1}{2 \sin 2\varphi} d\varphi \tag{12}$$

Using Eqs. (11) and (12) and calculating the magnitude $Q_{i\varphi}$ by Eq. (5), the contributions of different impact angles on fragmentation yield can be estimated (Fig. 8). The maximum yield for the C_{58}^+ fragment is at $\varphi = 0.75$ rad and for C_{56}^+ at $\varphi = 0.7$ rad. While this is a rough estimate, it has the right behavior, and is in qualitative agreement with the experimental shifts.

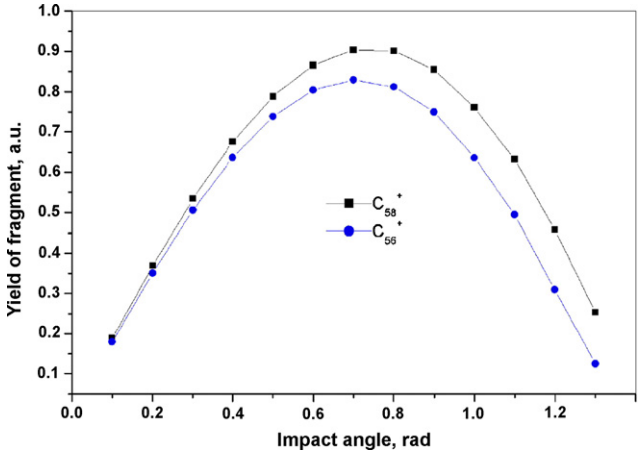

Fig. 8. Fragmentation yield ($C_{58}^+$and C_{56}^+) vs. impact angle φ at a constant restitution coefficient k_1.

5. Conclusions

The tandem (TOF/TOF) time-of-flight mass spectrometer provides a unique opportunity to evaluate collision energetics and mechanisms based on the small differences in arrival times of the product ions that reflect the partitioning of the initial collision energy into the kinetic and internal energy of the target and products. The curved-field reflectron is helpful for this approach in that it enables us to access very high collision energies, because it does not require reacceleration of the product ions after collision to accommodate the more limited bandwidths of single- and dual-stage reflectrons. On the other hand it is necessary to model the field of this reflectron carefully, as we have described above using a semi-empirical approach, to predict ion arrival times that reflect collisions occurring at a specific location in the flight tube. Using this approach we find that relatively low energy collisions of fullerene C_{60}^+ with helium, around 4–8 keV, produce adducts with helium $C_{2n}He^+$ and even carbon fragments whose apparent mass shifts can be explained as products of direct elastic collision processes, but are also consistent with ICT theory in which a first elastic collision with a portion of the fullerene molecule m_a is followed by a fully inelastic collision. Collisions with neon at 6 keV resulted in relatively small shifts in arrival times (reported as shifts in apparent mass) that suggested a modified ICT model that included a first (at least partially) inelastic step that resulted in much smaller to the kinetic energies of the fragments. The combination of higher relative energy with a neon target and the lower ionization potential and upper electronic states for neon suggests that this step may involve conversion into the internal (electronic) energy of the target. ICT mechanisms that include a knockout of the colliding partner (most likely C_2) can also contribute to this process. At laboratory collision energies of 20 keV, the modified ICT models suggest that there is sufficient energy in a second fully inelastic interaction between m_a and the rest of the fullerene ion for abundant fragmentation to occur over a wide range of impact angles and inelasticity in the first encounter. For low impact angle collisions (nearly head-on) the energy transfer at very high collision energies is results in the production of lower mass C_n^+ fragments.

Acknowledgements

This work was supported by a grant to RJC (GM64402) from the National Institutes of Health and a contract (N01 HV28180) to J. Van Eyk from the National Heart Lung and Blood Institute.

Appendix A

For a linear reflectron ($a = 0$), the expressions of TOF are the most clear for head on collisions. Specifically, one may determine the TOF of metastable products [37] by substituting the velocities $V_{p,m} = V_0$ and energies $T_{p,m} = T_0(M - m_n)/M$ for metastable ions into Eq. (10) to determine the time in the CFR and then computing the total time $t_{p,m}$ from the relationship

$t = t_{acc} + L/V + t_{CFR}$:

$$t_{p,m} = \frac{L}{V_0} + \frac{2}{eE}\left[2T_0\frac{(M-m_n)^2}{M}\right]^{1/2} = \frac{L}{V_0} + 4\frac{d_0}{V_0} - 4\frac{d_0}{V_0}\frac{m_n}{M} \quad (A1)$$

where d_0 is the reflectron penetration depth of the parent ion with energy T_0, E the electric field strength ($E = T/d$), and the very short time t_{acc} is omitted for simplicity. Similarly, if the collision takes place at a point C in the drift space (the location of the collision chamber), one can determine the TOF for the fragments following an elastic collision:

$$t_{p,elastic} = \frac{C}{V_0} + \frac{L-C}{V} + \frac{2}{eE}\left[2T_0\frac{(M-m_n)^2}{M}\left(\frac{M-m_g}{M+m_g}\right)^2\right]^{1/2} = t_1 + 2\frac{L-C}{V_0}\frac{m_g}{M-m_g} - 8\frac{d_0}{V_0}\frac{m_g}{M+m_g}\left(1-\frac{m_n}{M}\right) \quad (A2)$$

In the case of inelastic collisions fragment ions are generated with flight times:

$$t_{p,inelastic} = \frac{C}{V_0} + \frac{L-C}{V_0}\frac{M+m_g}{M} - \frac{2}{eE}\left[2T_0M\left(\frac{M+m_g-m_n}{M+m_g}\right)^2\right]^{1/2} = \frac{L}{V_0} + \frac{L-C}{V_0}\frac{m_g}{M} - \frac{4d_0}{V_0}\frac{M+m_g-m_n}{M+m_g} \quad (A3)$$

The fragment may or include the target gas (or a portion of the target gas in the case of a molecular target). Specifically in the case of fullerene with helium two different species: C_nHe^+ or $C_n{}^+$ would be possible. Using the appropriate mass m_n for the leaving neutral the flight time for a fragment ion incorporating helium C_nHe^+:

$$t_{pHe,inelastic} = \frac{L}{V_0} + 4\frac{d_0}{V_0} - 4\frac{d_0}{V_0}\frac{m_n}{M+m_g} + \frac{L-C}{V_0}\frac{m_g}{M} = t_1 + \frac{L-C}{V_0}\frac{m_g}{M} + 4\frac{d_0}{V_0}\frac{m_nm_g}{M^2} \quad (A4)$$

It should be noted that if intact precursor ion/helium complex does not dissociate ($m_n = 0$), the change in the flight time occurs in the drift time only; while the flight time in a linear reflectron is still the same as for a parent ion. If helium and m_n are released from the activated ion complex to form products of the type $C_n{}^+$, their flight times are

$$t_{p,inelastic} = \frac{L}{V_0} + \frac{L-C}{V_0}\frac{m_g}{M} - \frac{4d}{V_0}\frac{M+m_g-(m_n+m_g)}{M+m_g} = t_1 + \frac{L-C}{V_0}\frac{m_g}{M} - \frac{4d}{V_0}\frac{m_g}{M}\left(1-\frac{m_n}{M}\right) \quad (A5)$$

If fragments are formed according to ICT the TOF of the fragment ion has a simple result when the impact angle $\varphi = 0$:

$$t_{p,ICT} = \frac{C}{V_0} + \frac{L-C}{V_0}\frac{M(m_g+m_a)}{M(m_g+m_a)-2m_gm_a} + \frac{4d_0}{V_0}\frac{(M(m_g+m_a)-2m_gm_a)(M-m_n)}{M^2(m_g+m_a)} = t_1 + \frac{L-C}{V_0}\frac{2m_gm_a}{M(m_g+m_a)-2m_gm_a} - \frac{8d_0}{V_0}\frac{m_gm_a(1-m_n/M)}{M(m_g+m_a)} \quad (A6)$$

Appendix B

B.1. Partially elastic impact

A more detailed analysis would distinguish different types of excitation in each step of the collision process. Thus, the first step in ICT theory might also be considered as an elastic–inelastic or partially elastic impact. It is convenient to characterize this type of interaction by a restitution coefficient k that depends upon the molecular structure and ranges from 1 to 0 [28]. That is: in an elastic impact k equals 1; in an inelastic collision to 0. For an off centered impact between two hard spheres m_a and m_g (a velocity vector V_a does not coincide with the line of the impact) the velocity component V_{an0} on the impact line AT (Fig. 2, at $t = 0$) becomes:

$$V_{an} = \frac{(m_a - km_g)V_{an0}}{m_a+m_g} \quad (A7)$$

while the tangential components are not changed. Here, $V_{an0} = V_{a0}\mathrm{Cos}\varphi$. The increase of the internal energy of the particles is

$$\Delta Q_{a+g} = (V_{an} - V_{an0})^2\frac{(1-k^2)m_am_g}{2(m_g+m_a)} \quad (A8)$$

The restitution parameter is unknown, but might be determined empirically by evaluating experimental data for shifts in arrival times in line with this model.

References

[1] R.G. Cooks, Collision Spectroscopy, Plenum Press, NY, 1978.
[2] K.A. Shukla, J.H. Futrell, J. Mass Spectrom. 35 (2000) 1069.
[3] V. Karoly, J. Mass Spectrom. 31 (1996) 445.
[4] B. Spengler, D. Kirsch, R. Kaufmann, J. Phys. Chem. 96 (1992) 9678.
[5] G.F. Wells, C.E. Melton, Rev. Sci. Instrum. 28 (1957) 1065.
[6] D.L. Bricker, D.H. Russell, J. Am. Chem. Soc. 108 (1986) 6174.
[7] C.D. Bradley, J.M. Curtis, P.J. Derrick, B. Wright, Anal. Chem. 64 (1992) 2628.
[8] M.L. Gross, K.B. Tomer, R.L. Cerny, D.E. Giblin, FAB and tandem MS for structure determination of biomolecules success to M/Z 2000 and prospects for higher mass, in: C.J. McNeal (Ed.), Mass Spectrometry Analysis of Large Molecules, Wiley & Sons, UK, 1986, p. 171.
[9] E. Uggerud, P.J. Derrick, J. Phys. Chem. 95 (1991) 1430.
[10] K.A. Caldwell, D.E. Giblin, M.L. Gross, J. Am. Chem. Soc. 114 (1992) 3743.

[11] T. Weiske, D.K. Böhme, J. Hrušák, W. Krätschmer, H. Schwarz, Angew. Chem. Int. Ed. (English) 30 (1991) 884.
[12] M. Ross, J.H. Callahan, J. Phys. Chem. 95 (1991) 5720.
[13] R.C. Mowrey, M.M. Ross, J.H. Callahan, J. Phys. Chem. 96 (1992) 4755.
[14] Z. Wan, J.F. Christian, Y. Basir, S.L. Anderson, J. Chem. Phys. 99 (1993) 5570.
[15] H. Sprang, A. Mahlkow, E.E.B. Campbell, Chem. Phys. Lett. 227 (1994) 91.
[16] R.M. Ehlich, M. Westerburg, E.E.B. Campbell, J. Chem. Phys. 104 (1996) 1900.
[17] Y. Basir, S.L. Anderson, J. Chem. Phys. 107 (1997) 8370.
[18] D.E. Giblin, M.L. Gross, M. Saunders, J. Am. Chem. Soc. 119 (1997) 9880.
[19] R. Ehlich, O. Knospe, R. Schmidt, J. Phys. B: Atom. Mol. Opt. Phys. 30 (1997) 5429.
[20] E.E.B. Campbell, R. Ehlich, G. Heusler, O. Knospe, H. Sprang, Chem. Phys. 239 (1998) 299.
[21] E.E.B. Campbell, Fullerene Collision Reaction, Kluwer Academics, Dordrecht, 2003.
[22] A. Itoh, H. Tsuchida, T. Majima, S. Anada, A. Yogo, N. Imanishi, Phys. Rev. A 61 (1999) 1, 12702.
[23] S. Tomita, P. Hvelplund, S.B. Nielsen, Phys. Rev. A 65 (2002) 1.
[24] L. Becker, R.J. Poreda, T.E. Bunch, Proc. Natl. Acad. Sci. 97 (2000) 2979.
[25] R.J. Cotter, S. Iltchenko, D. Wang, Int. J. Mass Spectrom. 240 (2005) 169.
[26] R.J. Cotter, B.D. Gardner, S. Iltchenko, R.D. English, Anal. Chem. 76 (2004) 1976.
[27] R.J. Cotter, S. Iltchenko, D. Wang, R. Gundry, J. Mass Spectrom. Soc. Japan 53 (2005) 7.
[28] W. Goldthmith, Impact. The Theory and Physics of Behaviour of Colliding Solids, Edward Arnold Ltd., London, 1960.
[29] A.A. Makarov, E.N. Raptakis, P.J. Derrick, Int. J. Mass Spectrom. Ion Process. 146–147 (1995) 165.
[30] B. Spengler, R.J. Cotter, Anal. Chem. 62 (1990) 793.
[31] R.C. Beavis, B.T. Chait, Chem. Phys. Lett. 181 (1991) 479.
[32] L. Balazs, A. Vertes, Anal. Chem. 63 (1991) 314.
[33] J. Zhou, W. Ens, K.G. Standing, A. Verentchikov, Rapid Commun. Mass Spectrom. 6 (1992) 671.
[34] P. Juhasz, M.L. Vestal, S. Martin, J. Am. Soc. Mass Spectrom. 8 (1997) 209.
[35] S. Berkenkamp, C. Menzel, F. Hillenkamp, K. Dreisewerd, J. Am. Soc. Mass Spectrom. 13 (2002) 209.
[36] Y. Wu, J. Wang, H. Fu, Y. Li, D. Yang, Microchem. J. 48 (1993) 29.
[37] R.J. Cotter, Time-of-Flight Mass Spectrometry: Instrumentation and Applications In Biological Research, American Chemical Society, Washington, DC, 1997.